

Supramolecular Nanomaterials

Supramolecular Engineering of Oligothiophene Nanorods without Insulators: Hierarchical Association of Rosettes and Photovoltaic Properties

Shiki Yagai,^{*[a, e]} Mika Suzuki,^[a] Xu Lin,^[a] Marina Gushiken,^[a] Takuya Noguchi,^[a] Takashi Karatsu,^[a] Akihide Kitamura,^[a] Akinori Saeki,^[c] Shu Seki,^[c] Yoshihiro Kikkawa,^[d] Yuki Tani,^[b] and Ken-ichi Nakayama^[b, e]

Abstract: Supramolecular rosettes of oligothiophenes that do not bear long aliphatic tails have been designed as semiconducting nanomaterials for solution-processable bulk heterojunction solar cells. The rosettes consist of six barbiturated thiényl[oligo(hexylthiophene)] units (Bar-T-hT_n; n = 3,4,5) aggregated by multiple hydrogen bonds, which have been directly visualized by scanning tunneling microscopy (STM) at a solid–liquid interface. ¹H NMR spectroscopy in [D₈]toluene showed that Bar-T-hT_n exists as a mixture of monomers and small hydrogen-bonded aggregates. Hierarchical organization of the hydrogen-bonded aggregates

took place through π–π stacking interactions upon casting their toluene solutions, resulting in the growth of highly ordered nanorods whose widths are consistent with the diameters of the rosettes. The nanorods could be generated in the presence of soluble fullerene derivatives via solution casting or the annealing of the resulting thin films. The solar cells fabricated based on these bulk heterojunction films showed power conversion efficiencies of 1–3%, which are far higher than those of the non-hydrogen-bonded reference oligothiophene and the derivative that possesses long aliphatic tails.

Introduction

Hierarchical formation of well-defined nanostructures from synthetically accessible small molecules through programmed self-assembly would be a cost-effective approach toward the fabrication of printable, large-area molecular devices. Columnar nanostructures spontaneously formed by discoid or star-shaped π-conjugated small molecules are particularly attractive nanostructures as media for the quasi-one-dimensional transport of charge carriers.^[1] Supramolecular chemists have ex-

plored the construction of such columnar nanostructures by supramolecular macrocyclization of heterocyclic small molecules directed by multiple hydrogen bonds.^[2] However, despite vast examples of successful construction of such hierarchically organized columnar nanostructures, little progress has been made toward their application in organic devices, especially in solution-processable bulk heterojunction (BHJ) solar cells.^[3–5] This lack of progress is partly due to the fact that the formation of thermodynamically stable supramolecular macrocyclic assemblies (rosettes)^[6] requires “electronically inactive” long aliphatic chains to avoid irreversible (phase-separated) aggregation,^[7] which can generate kinetically trapped assemblies.^[8] Such long aliphatic chains covering the semiconducting internal structure may hamper efficient charge separation with the n-type semiconductor and charge transportation between the nanostructures in BHJ films. Thus, the proper design of rosette-forming π-conjugated small molecules with sufficient solubility in organic media is necessary to afford highly organized nanostructures applicable to BHJ solar cells, while minimizing the unfavorable effects of the solubilizing chains on the electronic properties of the devices.

We have previously demonstrated that the barbiturate unit is a powerful functional group for the organization of various π-conjugated units into unique nanostructures. A variety of nanostructures such as rods,^[9] rings,^[9b, 10] coils,^[10] and interlocked rings (catenanes)^[11] have been obtained upon the coupling of a barbiturate group with π-conjugated units whose one end is equipped with a tridodecyloxyphenyl aliphatic tail

[a] Prof. Dr. S. Yagai, M. Suzuki, Dr. X. Lin, M. Gushiken, T. Noguchi,

Prof. Dr. T. Karatsu, Prof. Dr. A. Kitamura

Department of Applied Chemistry and Biotechnology

Graduate School of Engineering, Chiba University

1-33 Yayoi-cho, Inage-ku, Chiba 263-8522 (Japan)

Fax: (+81)43-290-3039

E-mail: yagai@faculty.chiba-u.jp

[b] Y. Tani, Prof. Dr. K.-i. Nakayama

Graduate School of Science and Engineering, Yamagata University

1-1 Higashi, Tsukuba, Ibaraki 305-8562 (Japan)

[c] Prof. Dr. A. Saeki, Prof. Dr. S. Seki

Department of Applied Chemistry, Graduate School of Engineering

Osaka University, 2-1, Yamadaoka, Suita, Osaka 565-0871 (Japan)

[d] Dr. Y. Kikkawa

National Institute of Advanced Industrial Science and Technology (AIST)

1-1 Higashi, Tsukuba, Ibaraki 305-8562 (Japan)

[e] Prof. Dr. S. Yagai, Prof. Dr. K.-i. Nakayama

CREST, JST, Chiyoda-ku, Tokyo 102-0075 (Japan)

Supporting information for this article is available on the WWW under <http://dx.doi.org/10.1002/chem.201404428>.

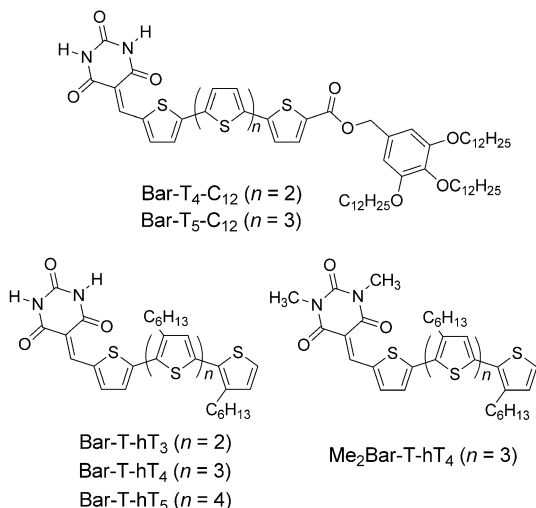


Figure 1. Chemical structures of $\text{Bar-T}_n\text{-C}_{12}$, Bar-T-hT_n and $\text{Me}_2\text{Bar-T-hT}_4$.

(for example, $\text{Bar-T}_4\text{-C}_{12}$ in Figure 1). For all of the prepared molecules, the formation of hexameric rosettes was proposed on the basis of X-ray diffraction analyses of their hexagonal or rectangular columnar mesophases, even though the literature contains no reports regarding the formation of supramolecular rosettes by barbiturates.^[12] Such a strong hydrogen-bond-mediated self-organization capability of barbiturate-conjugated π -systems motivated us to design supramolecular rosettes that can stack to form highly ordered nanorods applicable to solution-processable solar cells without the use of the long aliphatic tails.

Herein we report the synthesis, self-organization and photovoltaic properties of barbiturate-conjugated thiophene-[oligo(hexylthiophene)]s (Bar-T-hT_n ; $n = 3, 4, 5$ in Figure 1).^[13] In these molecules, solubilizing alkyl chains are grafted onto the π -conjugated backbone and thereby good solubilities of the resulting rosettes are guaranteed by the short alkyl chains embedded inside the rosettes (Figure 2 a). These rosettes without exterior aliphatic tails are anticipated to self-assemble through stacking into nanorods with electronically active surfaces (Figure 2 b). We demonstrate the hierarchical self-assembly process of these compounds from rosettes to highly ordered nanorods. By comparing the photovoltaic properties of the BHJ solar cells using Bar-T-hT_n and soluble fullerene derivatives, we disclose that the particular self-organization behavior of Bar-T-hT_4 upon thermal annealing of its BHJ film plays an important role in achieving power conversion efficiency (PCE) greater than 3%. We further demonstrate the importance of the present molecular design to achieve high-performance supramolecular solar cells by comparison with $\text{Bar-T}_5\text{-C}_{12}$, which possesses long aliphatic tails, and the non-hydrogen-bonding derivative $\text{Me}_2\text{Bar-T-hT}_4$ (Figure 1).

Results and Discussion

Synthesis

Bar-T-hT_n systems were synthesized as outlined in Scheme 1. The starting material for the synthesis of Bar-T-hT_n was stannyl-

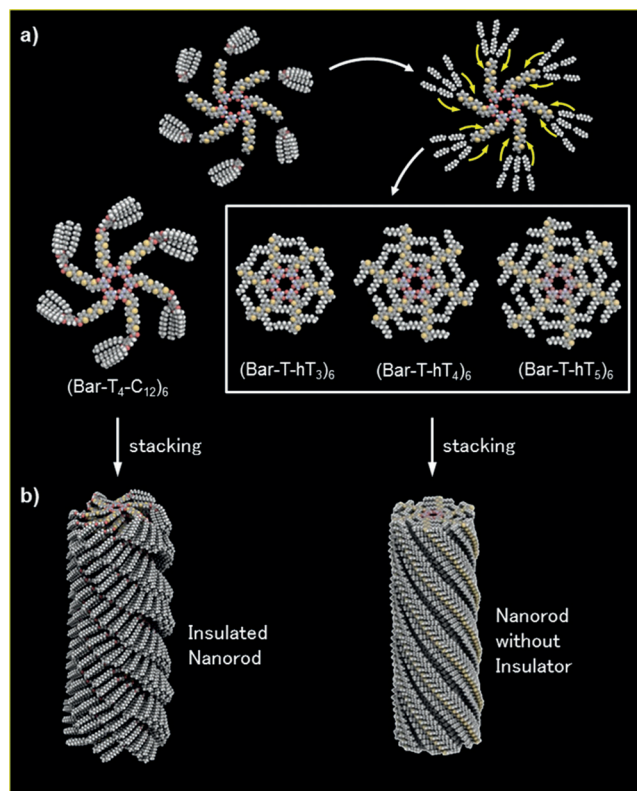
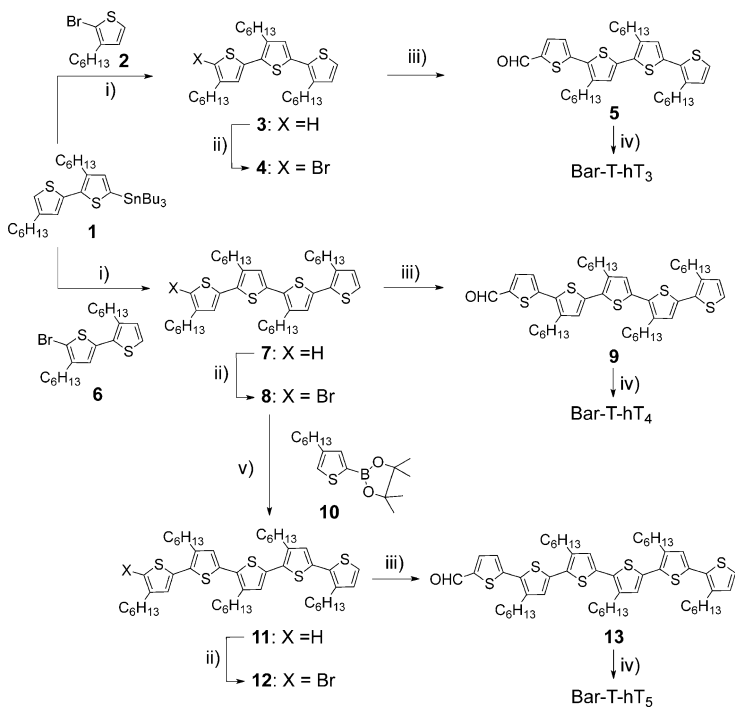


Figure 2. a) Design concept of oligothiophene rosettes in this study. CCW rosettes of $\text{Bar-T}_4\text{-C}_{12}$ (left) and Bar-T-hT_n are shown (see text). b) Schematic representation of nanorods of $\text{Bar-T}_4\text{-C}_{12}$ (left) and Bar-T-hT_n (right).

bithiophene **1**,^[14] which reacted with bromothiophene **2** or bromobithiophene **6** under Stille coupling conditions to give terthiophene **3** and quaterthiophene **7**, respectively. After selective monobromination^[15] of **3** and **7** using *N*-bromosuccinimide (NBS), the resulting species, **4** and **8**, underwent Suzuki coupling reactions with 5-formylthiophene-2-boronic acid to give **5** and **9**, respectively. For **8**, further thienylation was achieved by coupling with **10** to give **11**. After monobromination of **11** with NBS, the resulting **12** was also coupled with 5-formylthiophene-2-boronic acid to give **13**. The formyloligothiophenes **5**, **9**, and, **13** were treated with barbituric acid under neutral condition to give Bar-T-hT_3 , Bar-T-hT_4 , and Bar-T-hT_5 , respectively. The non-hydrogen-bonding derivative $\text{Me}_2\text{Bar-T-hT}_4$ was also prepared by the reaction of **9** with *N,N'*-dimethylbarbituric acid. These compounds were purified by recycling gel-permeation chromatography, and characterized by ^1H and ^{13}C NMR spectroscopy and high-resolution mass spectrometry.

Characterization of Rosettes by STM

Our previous attempt to verify the formation of barbiturate rosettes by scanning tunneling microscopy (STM) analysis of $\text{Bar-T}_4\text{-C}_{12}$ at the liquid-solid interface^[16] failed because the rosette architecture of $\text{Bar-T}_4\text{-C}_{12}$ whose exterior is decorated with bulky aliphatic tails led to a considerable free interior volume (Figure 2 a), thus lowering its two-dimensional packing efficiency. However, Bar-T-hT_n designed in this study, can fill the free



Scheme 1. Synthesis of barbiturate-conjugated oligo(hexylthiophene) structures Bar-T-hT_n. Reagents and conditions: i) [Pd(PPh₃)₄], DMF, microwave, 140 °C; ii) NBS, CHCl₃/acetic acid, 0 °C → RT; iii) 5-formylthiophene-2-boronic acid, K₂CO₃, [Pd(dppf)Cl]₂, toluene/MeOH, 80 °C; iv) barbituric acid, EtOH, reflux; v) 10, K₂CO₃, [Pd(PPh₃)₄], toluene/H₂O, reflux.

volume upon rosette formation (Figure 2 a), and stabilization of the resulting rosettes at the liquid-solid interface is therefore anticipated. The two-dimensional self-assembly of Bar-T-hT_n was thus studied by STM at the solid-liquid interface between highly oriented pyrolytic graphite (HOPG) and 1-phenyloctane.

Figure 3 a shows a typical STM image of Bar-T-hT₅. Although the individual thiophene rings could not be resolved, the average length of the bright rods [2.85 ± 0.1 nm (mean \pm SD)] is close to the extended molecular length (calculated to be 2.87 nm using the CPK model). The windmill-shaped arrangement of the bright rods demonstrates the formation of hexameric rosette of Bar-T-hT₅. The unit-cell parameters, $a = 5.1 \pm 0.2$ nm, $b = 5.5 \pm 0.1$ nm, and $\gamma = 60 \pm 5^\circ$, indicate the formation of a pseudohexagonal lattice of rosettes. The oppositely located bright rods in a rosette are not on the same line across the center of the rosette, indicating the formation of screw-shaped chiral rosettes with CW (clockwise; Figure 3 c) and CCW (counterclockwise; Figure 3 d) rotations, as was observed for melamine-functionalized oligo(*p*-phenylenevinylene)s.^[16a,17] Molecular modelling showed that both CW and CCW rosettes of Bar-T-hT₅ could be packed into the hexagonal lattice of the STM images through interdigititation of the outer hexyl chains (Figure 3 b). Either CW or CCW domains were observed randomly for each 25×25 nm² scan, and we could not find a boundary between the two domains. More detailed discussion of hydrogen-bonding motif is given in the Supporting Information (Figure S1).

For Bar-T-hT₄, we could only obtain poorly resolved STM images of rosettes, even after varying the parameters and re-

peating the measurements (see the Supporting Information, Figure S2). The center-to-center distance between neighboring rosettes (corresponding to lattice parameters a and b) are in the range of 4–5 nm. This result indicates that rosettes of Bar-T-hT₄ have intrinsically low two-dimensional packing efficiencies, which could intuitively be related to its shorter π -conjugation length compared to that of Bar-T-hT₅. However, Bar-T-hT₃, for which the π -conjugation is further reduced, gave well-resolved images of two-dimensionally organized rosettes in a hexagonal motif ($a = 4.4 \pm 0.1$ nm, $b = 4.2 \pm 0.1$ nm, $\gamma = 63 \pm 3^\circ$; see the Supporting Information, Figure S3). These observations could be explained using molecular modeling to determine the two-dimensional packing of the CCW rosettes of Bar-T-hT₄ and Bar-T-hT₃ (see the Supporting Information, Figure S4). Whereas the rosettes of Bar-T-hT₃ can be packed with a minimum void space, those of Bar-T-hT₄ leave notable void spaces surrounded by three rosettes, which suggests that fewer intermolecular and molecule–substrate interactions occur per unit area in the case of Bar-T-hT₄. Thus, the STM studies of Bar-T-hT_n imply that whether there is an odd or even number of hexylthiophene units strongly affects the two-dimensional organization of the rosettes.^[18]

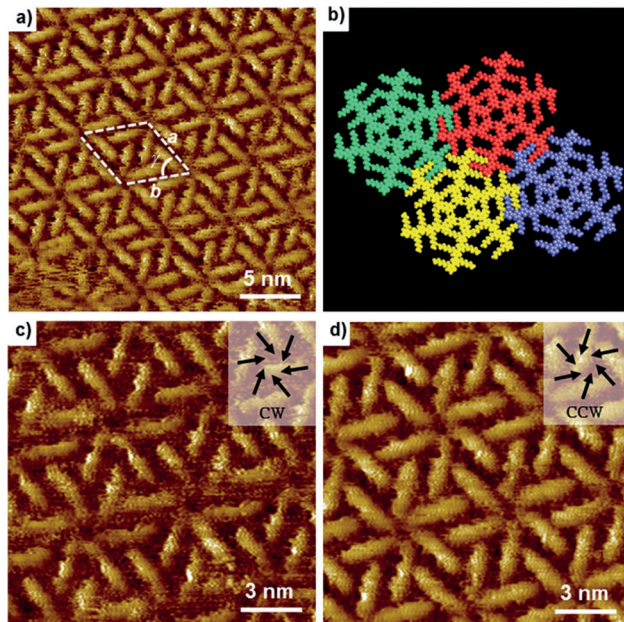


Figure 3. a) STM images of Bar-T-hT₅ (domain of CCW rosettes) at 1-phenyloctane-HOPG interface. The tunneling conditions: $I = 1.2$ pA, $V = -800$ mV. b) Packing model of the CCW rosette of Bar-T-hT₅ with the P/trans combination (see the Supporting Information). c,d) Magnification of STM images of c) CW and d) CCW rosettes.

¹H NMR Spectroscopy

Aggregation of Bar-T-hT_n was investigated by ¹H NMR spectroscopy in [D₆]toluene. Figure 4 a shows the change of ¹H NMR

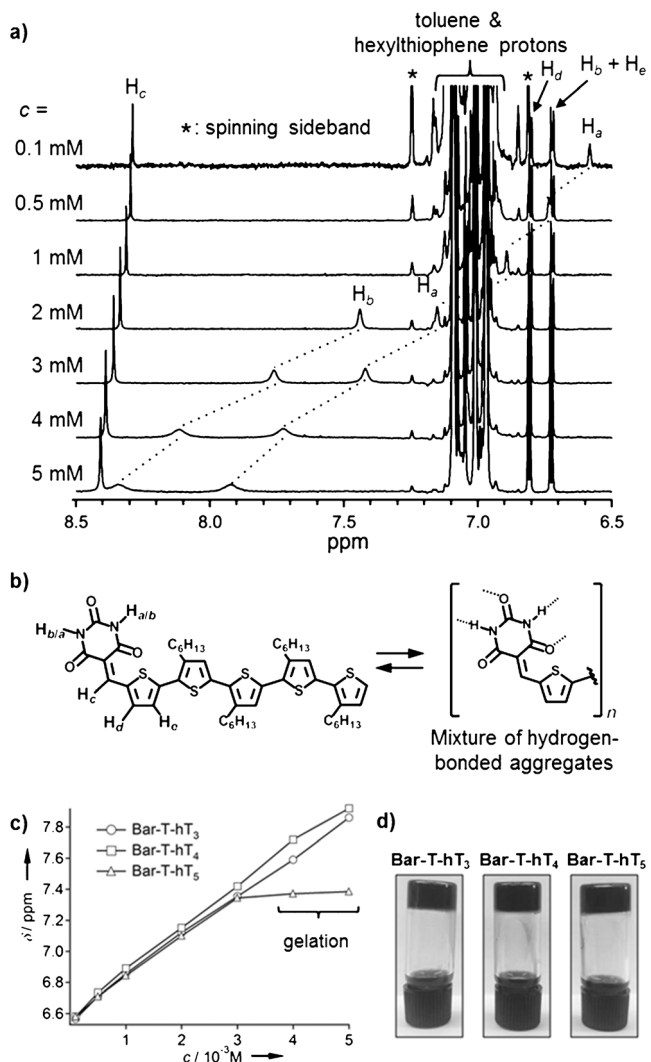


Figure 4. a) ^1H NMR spectra of Bar-T-hT₄ in [D₈]toluene at various concentrations. b) Assignments of proton signals a-e of Bar-T-hT₄. c) Plots of concentrations versus the chemical shift of a barbiturate proton (H_o) for Bar-T-hT₃ (○), Bar-T-hT₄ (□) and Bar-T-hT₅ (△). d) Toluene gels of Bar-T-hT₃ ($c=5\times 10^{-3}$ M), Bar-T-hT₄ ($c=5\times 10^{-3}$ M), and Bar-T-hT₅ ($c=4\times 10^{-3}$ M), obtained after 6 h on cooling homogeneous hot solutions.

spectra of Bar-T-hT₄ upon increasing the concentration from 1×10^{-4} to 5×10^{-3} M. At the lowest concentration, the signals of protons H_a and H_b of the barbiturate unit appeared at 6.58 and 6.80 ppm, respectively. On increasing concentration, these signals shifted downfield, which indicates the formation of intermolecular hydrogen bonds (Figure 4b). The $\Delta\delta$ values of H_a and H_b reached 1.34 ppm ($6.58 \rightarrow 7.92$ ppm) and 1.54 ppm ($6.80 \rightarrow 8.34$ ppm) at $c = 5 \times 10^{-3}$ M, respectively. The signal of the olefinic proton (H_c) also showed a small downfield shift ($\Delta\delta = 0.12$) due to deshielding by neighboring molecules. In sharp contrast, the protons of thiophene rings are all insensitive to the concentration change. These observations indicate that the molecules are in rapid equilibrium between the monomer and the hydrogen-bonded aggregates, and no hierarchical organization of the aggregates through $\pi-\pi$ stacking takes place under these conditions.

Bar-T-hT₃ also exhibited downfield shift of the barbiturate protons H_a and H_b upon increasing concentration (see the Supporting Information, Figure S5). On increasing the concentration from 1×10^{-4} M to 5×10^{-3} M, the $\Delta\delta$ values of H_a and H_b are 1.29 and 1.59 ppm (Figure 4c), respectively, which are comparable to those of Bar-T-hT₄. Bar-T-hT₅, in contrast, exhibited downfield shift of the barbiturate protons only up to 3×10^{-3} M, above which no significant shift was detected (see the Supporting Information, Figure S6). This was at first a puzzling observation, but we noticed that toluene solutions of Bar-T-hT₅ became viscous at this concentration range, and at above 4×10^{-3} M the solution immediately turned into a gel upon the heating-cooling procedure (Figure 4d). Scanning electron microscopy (SEM) of the dried gel showed the formation of entangled fibrous microstructures (see the Supporting Information, Figure S7). From these results, the absence of downfield shift above 3×10^{-3} M can be attributed to the saturation of Bar-T-hT₅ in toluene. With this result in hand, we revisited toluene solutions of Bar-T-hT₃ and Bar-T-hT₄, and found that they turned into gels within 6 h at 5×10^{-3} M at room temperature (Figure 4d). These results demonstrate that Bar-T-hT_n dissolved in toluene slowly aggregate to form microscopic fibers.

Formation of Nanorods

To study the hierarchical aggregation of Bar-T-hT_n into rodlike structures through the formation of rosettes, their diluted toluene solutions ($c < 1 \times 10^{-4}$ M), the ¹H NMR spectroscopy of which showed that the molecules are predominantly in molecularly-dissolved state, were deposited onto HOPG. After the solvent was slowly removed by evaporation, leading to the formation of aggregates, the resulting thin films were imaged by atomic force microscopy (AFM). When the samples were prepared from the solutions of $c = 5 \times 10^{-5}$ M, bundled nanorods were observed for Bar-T-hT₃ and Bar-T-hT₅, whereas granular nanoaggregates were observed for Bar-T-hT₄ (Figures 5a–c). These results demonstrate a weaker aggregation propensity of Bar-T-hT₄ in comparison to Bar-T-hT₃ and Bar-T-hT₅.

Upon increasing the concentrations of the solutions to 1×10^{-4} M, however, nanorods became observable for Bar-T-hT₄. Figures 5 d-f show typical high-resolution AFM images of bundled nanorods of Bar-T-hT_n with cross-sectional analyses along the white lines. The cross sectional analyses showed the zigzag patterns on the surface of bundled rods, and average top-to-top distances between neighboring rods were calculated as 4.1 nm for Bar-T-hT₃, 4.3 nm for Bar-T-hT₄, and 5.0 nm for Bar-T-hT₅, upon dividing the total top-to-top distance of the bundles by the number of aligned rods. Because the calculated distances for Bar-T-hT₃ and Bar-T-hT₅ are well matched with the shorter lattice parameters of the two-dimensionally organized rosettes, the lateral interaction (i.e., interdigitation) between rosettes would play an important role in the formation of nanorods. The average heights of the nanorods also increased incrementally with increasing number of the thiényl units, from Bar-T-hT₃ (2.8 ± 0.1 nm) to Bar-T-hT₄ (3.0 ± 0.2 nm), and to Bar-T-hT₅ (3.7 ± 0.1 nm), which is consistent with an edge-on arrangement of the rosette nanorods. Although no helical mor-

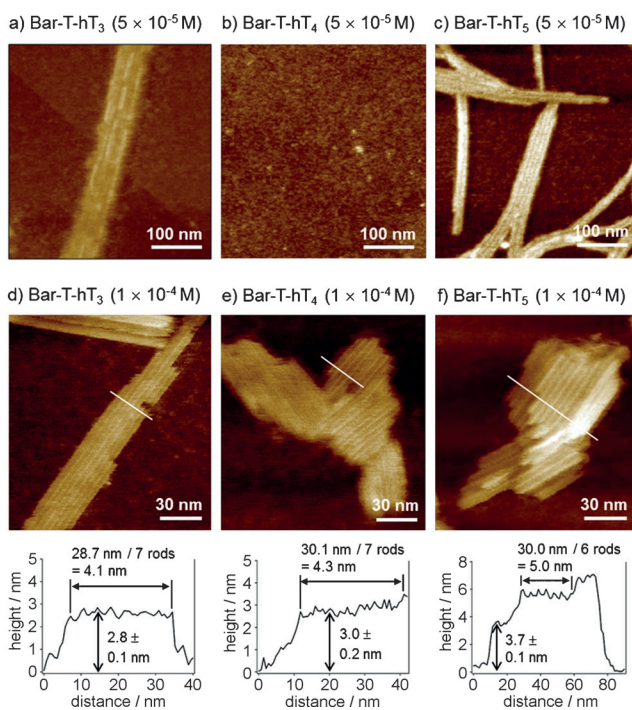


Figure 5. AFM images of thin films prepared by drop-casting toluene solutions of a,d) Bar-T-hT₃, b,e) Bar-T-hT₄ and c,f) Bar-T-hT₅ onto HOPG. Concentrations of the solutions are 5×10^{-5} M for images (a)–(c) and 1×10^{-4} M for images (d)–(f). For images (d)–(f), cross-sectional analysis along the white lines are shown below the images.

phology could be imaged for these nanorods by AFM, helical stacking of rosettes (Figure 2b) would be anticipated because offset stacking of oligothiophene π -conjugated moieties is favored by repulsive π – π interactions that is compensated by attractive π – σ interactions.^[19,20]

Optical and Electronic Properties

Monomeric Bar-T-hT_n in toluene gave rise to broad absorption bands in the range of 300–650 nm (Figure 6, Table 1), which are largely red-shifted by 100 nm compared to quinque-(hexyl)thiophene ($\lambda_{\text{max}} = 391$ nm).^[21] We thus anticipated that

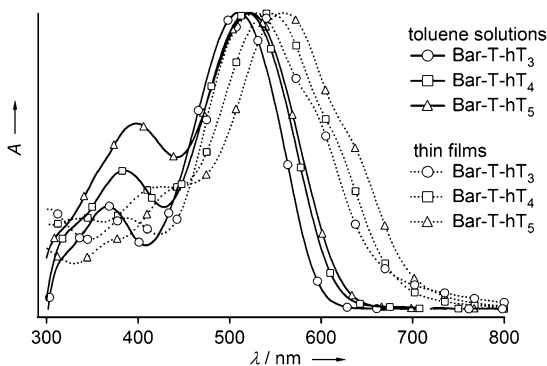


Figure 6. Absorption spectra of toluene solutions ($c = 1 \times 10^{-4}$ M, solid line) and thin films ($c = 1 \times 10^{-3}$ M, dotted line) of Bar-T-hT₃ (○), Bar-T-hT₄ (□) and Bar-T-hT₅ (△).

Table 1. Optical and electronic properties of Bar-T-hT_n.

Compound	$\lambda_{\text{max}}(\text{sol})$ [nm]	$\lambda_{\text{max}}(\text{film})$ [nm]	λ_{onset} [nm]	E_g [eV]	E_{HOMO} [eV]	E_{LUMO} [eV]
Bar-T-hT ₃	367, 508	386, 526	655	1.89	-5.18	-3.29
Bar-T-hT ₄	385, 520	418, 542	674	1.84	-5.06	-3.22
Bar-T-hT ₅	398, 522	538, 560	696	1.78	-4.96	-3.18

our oligothiophenes should have charge-transfer character in their excited state, owing to the strong electron-withdrawing effect of the barbiturate unit. The absorption maxima of Bar-T-hT₄ ($\lambda_{\text{max}} = 520$ nm) and Bar-T-hT₅ ($\lambda_{\text{max}} = 522$ nm) are slightly red-shifted compared to that of Bar-T-hT₃ ($\lambda_{\text{max}} = 508$ nm). The absorption bands of the solid films of Bar-T-hT_n displayed red-shifts of absorption maxima and emergence of new absorption shoulder in the longer wavelength region, and the red-shifted values increased upon increasing conjugation length (Bar-T-hT₃: $\Delta\lambda = 18$ nm; Bar-T-hT₄: $\Delta\lambda = 21$ nm; Bar-T-hT₅: $\Delta\lambda = 39$ nm). The red-shift and the absorption shoulder can be attributed to the coplanarization and π – π stacked aggregation of π -conjugated systems,^[22] respectively. The optical band gaps of the films were determined from the onset of absorption in the range from 1.78 to 1.89 eV (Table 1).

Cyclic voltammetry (CV) measurements of the thin film samples showed that Bar-T-hT₃, Bar-T-hT₄ and Bar-T-hT₅ have HOMO energy levels of -5.18, -5.06 and -4.96 eV, respectively. From the optical band gaps and these HOMO energy levels, LUMO energy levels of Bar-T-hT₃, Bar-T-hT₄ and Bar-T-hT₅ were estimated to be -3.29, -3.22, and -3.18 eV, respectively (Table 1). These energy levels demonstrate that Bar-T-hT_n species can be used as electron donor materials for BHJ solar cells with PC₆₁BM ([6,6]-phenyl-C₆₁-butyric acid methyl ester) or PC₇₁BM as electron acceptors.^[23]

Photovoltaic Properties

Photovoltaic properties of Bar-T-hT_n were investigated by fabricating BHJ solar cells with a structure of Al/Ca/Bar-T-hT_n:PC₆₁BM/PEDOT:PSS/ITO (Figure 7a) (PEDOT:PSS, poly(3,4-ethylenedioxythiophene)-poly(styrenesulfonate), as the hole injection layer; ITO, indium tin oxide, as the transparent electrode). Because Bar-T-hT_n species form gel-like materials in pure toluene at concentrations above 5 mg mL^{-1} , as described previously, we employed the 1:1 (v/v) mixture of chloroform and toluene as a solvent for the preparation of active layers (denoted as, e.g., Bar-T-hT₃:PC₆₁BM). The active layers were prepared by spin-coating the 1:1 (w/w) blends of Bar-T-hT_n and PC₆₁BM dissolved in the mixed solvents. Optimum thicknesses of the active layers were found to be in the range of 60–80 nm, which could be made with the total concentration of the materials of 10 mg mL^{-1} . The devices were fabricated using as-cast or thermally annealed (50, 80 and 110 °C) active layers to study the impact of thermal organization of nanorods.

Table 2 summarizes short-circuit current density (J_{sc}), open-circuit voltage (V_{oC}), fill factor (FF) and PCE of the BHJ solar cells fabricated using Bar-T-hT₃:PC₆₁BM, Bar-T-hT₄:PC₆₁BM and

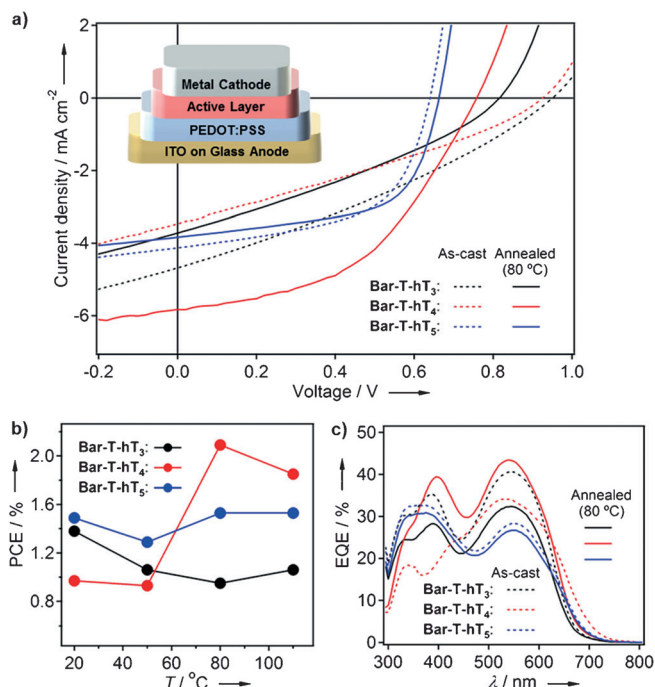


Figure 7. a) Current–voltage (J – V) characteristics of BHJ solar cells using 1:1 (w/w) blend films of Bar-T-hT₃:PC₆₁BM (black lines), Bar-T-hT₄:PC₆₁BM (red lines) and Bar-T-hT₅:PC₆₁BM (blue lines) before (dotted lines) and after annealing at 80 °C (solid lines). Inset: schematic representation of the device structure of the BHJ solar cells applied in this study. b) Plots of annealing temperatures versus PCE of the devices of Bar-T-hT₃ (black line), Bar-T-hT₄ (red line) and Bar-T-hT₅ (blue line). c) EQE spectra of the devices of Bar-T-hT₃ (black line), Bar-T-hT₄ (red line) and Bar-T-hT₅ (blue line) before (dotted lines) and after annealing at 80 °C (solid lines).

Table 2. Photovoltaic properties of the BHJ solar cells based on Bar-T-hT_n as donor and PC₆₁BM (annealing at as-cast, 50, 80, and 110 °C) or PC₇₁BM^[a] (annealing at only 80 °C) as acceptor under the illumination of AM 1.5 G (100 mW cm⁻²).

BHJ films	Annealing T [°C]	V_{oc} [V]	J_{sc} [mA cm ⁻²]	FF [%]	PCE [%]
Bar-T-hT ₃ :PC ₆₁ BM	as-cast	0.95	4.68	31.0	1.38
	50	0.82	4.23	30.6	1.06
	80	0.82	3.72	31.4	0.95
	110	0.77	3.66	37.3	1.06
Bar-T-hT ₃ :PC ₇₁ BM ^[a]	80	0.75	5.04	34.5	1.31
Bar-T-hT ₄ :PC ₆₁ BM	as-cast	0.93	3.47	30.1	0.97
	50	0.75	3.58	30.8	0.83
	80	0.76	5.83	47.2	2.09
	110	0.70	5.72	47.1	1.85
Bar-T-hT ₄ :PC ₇₁ BM ^[a]	80	0.79	7.00	54.4	3.01
Bar-T-hT ₅ :PC ₆₁ BM	as-cast	0.64	4.13	56.2	1.49
	50	0.61	4.19	50.3	1.29
	80	0.66	3.84	60.2	1.53
	110	0.66	3.75	62.4	1.53
Bar-T-hT ₅ :PC ₇₁ BM ^[a]	80	0.69	3.50	57.3	1.38

[a] A 9:1 (v/v) mixture of chloroform and toluene was used for the preparation of active layers.

Bar-T-hT₅:PC₆₁BM. Figure 7a represents the J – V curves of the devices using the as-cast and 80 °C-annealed active layers. All the devices displayed typical diode behaviors. Bar-T-hT₅ provid-

ed the best annealing-free device, giving a PCE of 1.49% with a J_{sc} of 4.13 mA cm⁻², a V_{oc} of 0.64 V, and a FF of 56.2%. Although the annealing-free device of Bar-T-hT₃ showed a higher J_{sc} (4.68 mA cm⁻²) and V_{oc} (0.95 V) compared to those of Bar-T-hT₅, its lower FF of 31% resulted in a lower PCE of 1.38%. Remarkably, Bar-T-hT₄, which has a π -conjugation length between those of Bar-T-hT₃ and Bar-T-hT₅, showed even lower J_{sc} (3.47 mA cm⁻²) and FF (30.1%) values than those of Bar-T-hT₃, thus giving the lowest PCE (0.97%) among the annealing-free devices.

In Figure 7b, PCEs of the solar cells of Bar-T-hT_n are plotted versus annealing temperature applied for the active layers. The devices of Bar-T-hT₃ and Bar-T-hT₅ showed only a small increase or decrease of PCEs upon increasing annealing temperature mainly due to the decrease of J_{sc} . Interestingly, the devices of Bar-T-hT₄ showed a pronounced improvement of the performance upon increasing the annealing temperature from 50 to 80 °C: J_{sc} increased from 3.58 to 5.83 mA cm⁻², FF increased from 30.8 to 47.1%, and PCE increased from 0.83 to 2.1%. Further elevating annealing temperature to 110 °C reduced the device performance. In most small-molecular solar cells using PC₆₁BM, thermal annealing at a temperature in the range of 100–130 °C has had a notable effect on the device performance,^[24–26] because the glass transition of PC₆₁BM promoted favorable phase separation to form semiconducting channels.^[27] The peculiar increase of PCE in the devices of Bar-T-hT₄ on applying a relatively moderate annealing temperature is a characteristic feature of the organization of Bar-T-hT₄, which is revealed by the AFM studies described in the next section. Further improvements in the device performance were achieved for Bar-T-hT_n by using PC₇₁BM as an acceptor (Table 2, gray lines), whose reduced symmetry leads to a stronger absorption in the visible region compared to that of PC₆₁BM.^[28] Also in this case the highest performance was that with Bar-T-hT₄, for which the PCE was 3.01% ($J_{sc}=7.00$ mA cm⁻², $V_{oc}=0.79$ V, FF=0.54). To knowledge, this PCE is the highest value reported for a small-molecular material that organizes through specific hydrogen-bonding interactions,^[29] and is comparable to PCEs of BHJ solar cells constructed with discotic small molecules.^[30]

External quantum efficiency (EQE) spectra of the solar cells using as-cast and 80 °C-annealed films of Bar-T-hT₃:PC₆₁BM, Bar-T-hT₄:PC₆₁BM and Bar-T-hT₅:PC₆₁BM are shown in Figure 7c. The device of Bar-T-hT₃ showed a negative impact of annealing on EQE in the region between 500–600 nm (40.6→32.4% at 545 nm), which is the major absorption region of Bar-T-hT₃. The device of Bar-T-hT₅ showed a small increase of EQE (26.7→28.3% at 550 nm) upon annealing. In striking contrast, a pronounced increase of EQE was observed for the device of Bar-T-hT₄ (34.1→43.4% at 540 nm). These observations imply that contrasting thermal reorganization did occur in Bar-T-hT₃:PC₆₁BM and Bar-T-hT₄:PC₆₁BM, whereas in Bar-T-hT₅:PC₆₁BM a substantial phase separation would have already occurred even before annealing due to the strong aggregation propensity of Bar-T-hT₅, thus resulting in the negligible impact of annealing. In contrast, the opposite effect of the thermal annealing on photocurrent generation in Bar-T-hT₃ and Bar-T-hT₄ is

consistent with the temperature dependence of the PCEs of their devices (Figure 7b), which will be correlated with the morphology change of the BHJ films as described below.

Nanorod Formation in BHJ films

The morphology change of the BHJ films upon annealing was studied by AFM. Figure 8 shows the AFM topography images

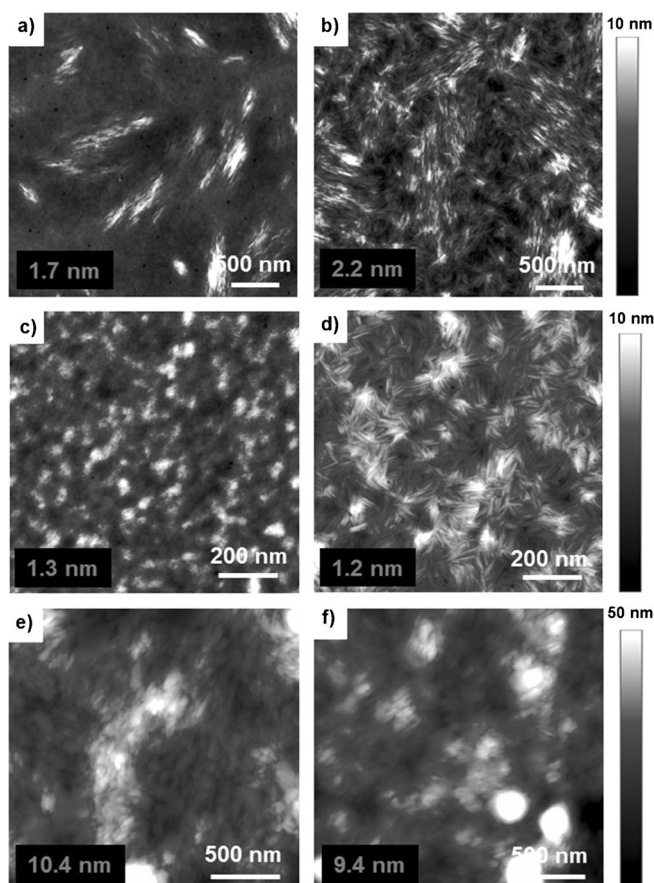


Figure 8. AFM topography images of the 1:1 (w/w) blend films of a,b) Bar-T-h₃:PC₆₁BM, c,d) Bar-T-h₄:PC₆₁BM and e,f) Bar-T-h₅:PC₆₁BM before (a,c,e) and after annealing at 80 °C (b,d,f). The values at the bottom-left corner are root-mean-square (RMS) roughness.

of the as-cast and annealed films of Bar-T-h₃:PC₆₁BM, Bar-T-h₄:PC₆₁BM and Bar-T-h₅:PC₆₁BM with the values of root-mean-square (RMS) roughness. The AFM images of Bar-T-h₃:PC₆₁BM revealed that bundled nanorods are already formed in the as-cast state (Figure 8a), which upon annealing resulted in a further agglomeration of nanorods (Figure 8b). The agglomeration would cause a decrease in the BHJ interface, thus reducing the photocurrent generation. For Bar-T-h₅:PC₆₁BM, the substantial phase separation is suggested from a higher RMS roughness recorded already before annealing, and the situation could not be improved even after annealing (Figure 8e,f). This result reflects the trivial impact of thermal annealing on the improvement of the solar cell performance.

The most pronounced morphology change was observed for Bar-T-h₄:PC₆₁BM. Whereas no well-defined nanostructure was observed in the as-cast film (Figure 8c), the formation of nanorods, which are not extensively bundled in comparison to Bar-T-h₃:PC₆₁BM and Bar-T-h₅:PC₆₁BM, was observed after annealing at 80 °C (Figure 8d). The nanorods were approximately 100 nm in length and 5–10 nm in width, which corresponds to the formation of single-rosette columns. The dispersed nature of these nanorods was also confirmed by the absence of diffraction peaks derived from the two-dimensional ordering of nanorods in the powder X-ray diffraction measurement of the annealed film. Increasing the annealing temperature to 110 °C caused bundling (width ≈ 20 nm) and elongation (length ≈ 200 nm) of nanorods (see the Supporting Information, Figure S8). This observation is consistent with the drop in the device performance at this annealing temperature.

Impact of Nanorod Formation on Photovoltaic Properties

Because the performance of BHJ solar cells depends strongly on the charge-separation efficiency and transport of generated charge carriers, we studied the impact of supramolecular organization of Bar-T-h₄ on the photovoltaic properties by flash-photolysis time-resolved microwave conductivity (FP-TRMC), informative for the motion of photogenerated charge carriers before complete deactivation by charge recombination and/or trapping.^[31] To cancel the change in the absorbance of the films upon thermal treatment, the film thicknesses were kept more than 1 μm in order to absorb most of the incident photons.^[31c] Upon excitation of the as-cast BHJ films of Bar-T-h₄:PC₆₁BM with a laser pulse at 355 nm, a pronounced transient conductivity, given by $\phi\Sigma\mu$ (ϕ =photocarrier generation yield; $\Sigma\mu$ =sum of the mobilities of photogenerated charge carriers) was observed (Figure 9a). Upon annealing the films at 50, 80, and 110 °C, the maximum $\phi\Sigma\mu$ decreased gradually from $1.3 \times 10^{-4} \text{ cm}^2 \text{ V}^{-1} \text{ s}^{-1}$ to $0.8 \times 10^{-4} \text{ cm}^2 \text{ V}^{-1} \text{ s}^{-1}$. The decrease of $\phi\Sigma\mu$ is attributable to a reduction in the charge carrier generation efficiency by the growth of the nanorods, which should lead to a decrease in the *p*-*n* heterojunction interface. In contrast, the half-decay-time ($\tau_{1/2}$) of the TRMC signals increased from $2.4 \times 10^{-6} \text{ s}$ to $10.1 \times 10^{-6} \text{ s}$ upon annealing at higher temperatures (Figure 9a, inset). These results demonstrate that neither insufficient nor excessive thermal annealing simultaneously guarantees efficient charge separation and transport (Figure 9b). Owing to this trade-off relationship of the nanorod growth for optimizing OPV output, the best performance was achieved when the BHJ films of Bar-T-h₄:PC₆₁BM were annealed at 80 °C.

Effect of Aliphatic Tails and Rosette Formation

To shed more light on our design concept toward supramolecular photovoltaic materials, we evaluated the photovoltaic properties of Bar-T₅-C₁₂ functionalized with long aliphatic tails, and Me₂Bar-T-h₄, hydrogen-bonding sites of which are capped with methyl groups. The 1:1 (w/w) blend of Bar-T₅-C₁₂ and PC₆₁BM gave good BHJ films owing to the presence of ali-

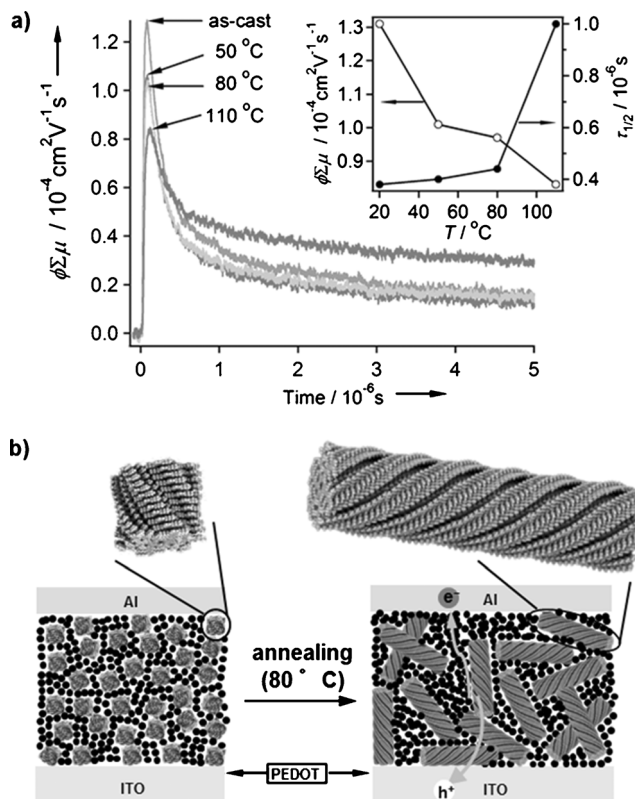


Figure 9. a) Conductivity transients ($\phi \Sigma \mu$) of the as-cast and annealed (50, 80 and 110 °C) blend films of Bar-T-hT₄:PC₆₁BM (1:1, w/w), observed upon excitation with a 355 nm laser pulse (excitation photon density = 9.1×10^{15} photons cm^{-2}). Inset: plot of $\phi \Sigma \mu$ and semi-log plot of $t_{1/2}$ versus the annealing temperatures. b) Schematic illustration of nanorod growth in the active layer and facilitation of charge carrier transportation.

phatic tails. However, its solar cells exhibited quite poor performance, as PCEs could be increased up to only 0.04% (Table 3). A significantly lower J_{sc} value (0.21 mA cm^{-2}) illustrates that the aliphatic tails hamper the charge separation with the acceptor material and charge carrier migration between nanorods.

Me₂Bar-T-hT₄ featuring a high solubility and optical and electrochemical properties almost comparable to those of Bar-T-hT₄ (see the Supporting Information, Table S2), also showed a poor solar cell performance. The 1:1 (w/w) blend of Me₂Bar-T-hT₄ and PC₆₁BM afforded BHJ films with very smooth surface

(RMS roughness = 0.5 nm) without the formation of well-defined nanostructures (see the Supporting Information, Figure S9a). However, its solar cells showed PCEs of only 0.1% with $J_{sc} = 2.89 \text{ mA cm}^{-2}$, $V_{oc} = 0.14 \text{ V}$, $FF = 24.7$ (Table 3). Thermal annealing at 80 °C was effective but it increased the PCE up to only 0.3%. The annealed film retained the structureless feature of the surface (RMS roughness = 1.0 nm, Figure S9b). The poor device performance and the structureless feature of the Me₂Bar-T-hT₄:PC₆₁BM system even after annealing thus unequivocally demonstrate that our supramolecular materials are effective for organizing small molecular semiconductors into well-defined hierarchical nanostructures without introducing long aliphatic tails.

Conclusion

The supramolecular design strategy applied herein enabled the construction of well-defined one-dimensional nanostructures through the hydrogen-bond-mediated supramolecular macrocyclization (rosette formation) of oligothiophene semiconductors without the use of long aliphatic tails. Due to the absence of exterior long aliphatic tails, the rosettes' two-dimensional packing efficiency at the liquid-solid interface was markedly affected by having an odd or even number of hexylthienyl groups. Interestingly, Bar-T-hT₄, which showed a lower two-dimensional packing efficiency of the rosette compared to Bar-T-hT₃ and Bar-T-hT₅, exhibited poorer organization propensity into nanorods. These results indicate that rosette-rosette interaction is important for the lateral interaction between the nanorods that promotes their growth. This property of Bar-T-hT₄ ensures good miscibility with the fullerene acceptor, and unbundled nanorods were formed in the BHJ films upon annealing, giving rise to a reasonable nanophasse-separated structure. The resulting BHJ structures of Bar-T-hT₄:PC₆₁BM exhibited photovoltaic properties comparable to those of the most commonly used standard polymer materials (P3HT).

Supramolecular macrocycles formed by multiple hydrogen-bonding interactions have long been explored as archetypal building modules for hierarchically organized columnar (rod-like) nanoarchitectures. Most soluble building blocks that afford these types of supermacrocyclic assemblies require long aliphatic tails to achieve sufficient solubility in organic solvents, which is important for avoiding the unfavorable precipitation of competing open-ended oligomers that are always in equilibrium with supermacrocyclic species to a small extent.^[7] Such long aliphatic tails, however, cover the resulting columnar nanostructures, thus diminish the photovoltaic activity of the materials. In our molecular design, however, the good solubility is imparted by short alkyl chains embedded inside the supramolecular macrocyclic structures. Thus, our hydrogen-bonded oligothiophenes can form well-defined nanorods that show, to our knowledge, the highest solar cell performance among hydrogen-bonded materials. Because the similar strategy might be applied not only to hydrogen-bonded building blocks but also to large star-shaped molecules, we hope that this study may open a new avenue for the design of supramolecular materials with not only well-defined nanoarchitec-

Table 3. Comparison of photovoltaic properties of the BHJ Solar Cells based on Bar-T-hT₄ or Bar-T₅-C₁₂ or Me₂Bar-T-hT₄ as donor and PC₆₁BM as acceptor under the illumination of AM 1.5 G (100 mW cm^{-2}).

BHJ films	Annealing T [°C]	V_{oc} [V]	J_{sc} [mA cm^{-2}]	FF [%]	PCE [%]
Bar-ThT ₄ :PC ₆₁ BM	as-cast	0.93	3.47	30.1	0.97
	80	0.76	5.83	47.2	2.09
Bar-T ₅ C ₁₂ :PC ₆₁ BM	as-cast	0.68	0.21	28.5	0.04
	80	0.78	0.14	27.1	0.03
Me ₂ Bar-T-hT ₄ :PC ₆₁ BM	as-cast	0.14	2.89	24.7	0.10
	80	0.16	7.89	24.9	0.32

tures and solution processability but also practical application in devices. Current work in our group is directed toward further improvement of device performance by engineering electronic and optical properties of molecular components, as well as controlling over the orientation of nanorods in the device.

Keywords: nanostructures · oligothiophene · photovoltaics · self-assembly · supramolecular chemistry

- [1] a) F. J. M. Hoeben, P. Jonkheijm, E. W. Meijer, A. P. H. J. Schenning, *Chem. Rev.* **2005**, *105*, 1491–1546; b) A. C. Grimsdale, K. Müllen, *Angew. Chem.* **2005**, *117*, 5732–5772; *Angew. Chem. Int. Ed.* **2005**, *44*, 5592–5629; c) S. Sergeyev, W. Pisula, Y. H. Geerts, *Chem. Soc. Rev.* **2007**, *36*, 1902–1929; d) S. Laschat, A. Baro, N. Steinke, F. Giessmann, C. Haegele, G. Scalia, R. Judele, E. Kapatsina, S. Sauer, A. Schreivogel, M. Tosoni, *Angew. Chem.* **2007**, *119*, 4916–4973; *Angew. Chem. Int. Ed.* **2007**, *46*, 4832–4887; e) A. L. Kanibolotsky, I. F. Perepichka, P. J. Skabar, *Chem. Soc. Rev.* **2010**, *39*, 2695–2728.
- [2] a) N. Kimizuka, T. Kawasaki, K. Hirata, T. Kunitake, *J. Am. Chem. Soc.* **1995**, *117*, 6360–6361; b) W. Yang, X. Chai, L. Chi, X. Liu, Y. Cao, R. Lu, Y. Jiang, X. Tang, H. Fuchs, T. Li, *Chem. Eur. J.* **1999**, *5*, 1144–1149; c) H. Fenniri, P. Mathivanan, K. L. Vidale, D. M. Sherman, K. Hallenga, K. V. Wood, J. G. Stowell, *J. Am. Chem. Soc.* **2001**, *123*, 3854–3855; d) P. Jonkheijm, A. Miura, M. Zdanowska, F. J. M. Hoeben, S. De Feyter, A. P. H. J. Schenning, F. C. De Schryver, E. W. Meijer, *Angew. Chem.* **2004**, *116*, 76–80; *Angew. Chem. Int. Ed.* **2004**, *43*, 74–78; e) S. Jin, Y. Ma, S. C. Zimmerman, S. Z. D. Cheng, *Chem. Mater.* **2004**, *16*, 2975–2977; f) S. Yagai, T. Nakajima, K. Kishikawa, S. Kohmoto, T. Karatsu, A. Kitamura, *J. Am. Chem. Soc.* **2005**, *127*, 11134–11139; g) A. Piermattei, M. Giesbers, A. T. M. Marcelis, E. Mendes, S. J. Picken, M. Crego-Calama, D. N. Reinhoudt, *Angew. Chem.* **2006**, *118*, 7705–7708; *Angew. Chem. Int. Ed.* **2006**, *45*, 7543–7546; h) S. Yagai, S. Mahesh, Y. Kikkawa, K. Unoike, T. Karatsu, A. Kitamura, A. Ajayaghosh, *Angew. Chem.* **2008**, *120*, 4769–4772; *Angew. Chem. Int. Ed.* **2008**, *47*, 4691–4694; i) S. Yagai, M. Usui, T. Seki, H. Murayama, Y. Kikkawa, S. Uemura, T. Karatsu, A. Kitamura, A. Asano, S. Seki, *J. Am. Chem. Soc.* **2012**, *134*, 7983–7994.
- [3] For reviews on BHJ solar cells, see: a) B. C. Thompson, J. M. J. Fréchet, *Angew. Chem.* **2008**, *120*, 62–82; *Angew. Chem. Int. Ed.* **2008**, *47*, 58–77; b) A. W. Hains, Z. Liang, M. A. Woodhouse, B. A. Gregg, *Chem. Rev.* **2010**, *110*, 6689–6735; c) J. L. Delgado, P.-A. Bouit, S. Filippone, M. A. Herranz, N. Martin, *Chem. Commun.* **2010**, *46*, 4853–4865; d) C. J. Brabec, M. Heeney, I. McCulloch, J. Nelson, *Chem. Soc. Rev.* **2011**, *40*, 1185–1199; e) G. Li, R. Zhu, Y. Yang, *Nat. Photonics* **2012**, *6*, 153–161; f) A. J. Heeger, *Adv. Mater.* **2014**, *26*, 10–28; g) Y. Huang, E. J. Kramer, A. J. Heeger, G. C. Bazan, *Chem. Rev.* **2014**, *114*, 7006–743.
- [4] For reviews on small-molecular BHJ solar cells, see: a) F. Würthner, K. Meerholz, *Chem. Eur. J.* **2010**, *16*, 9366–9373; b) A. Mishra, P. Bäuerle, *Angew. Chem.* **2012**, *124*, 2060–2109; *Angew. Chem. Int. Ed.* **2012**, *51*, 2020–2067; c) Y. Lin, Y. Li, X. Zhan, *Chem. Soc. Rev.* **2012**, *41*, 4245–4272; d) C. Li, H. Wonneberger, *Adv. Mater.* **2012**, *24*, 613–636; e) S. S. Babu, S. Prasanthkumar, A. Ajayaghosh, *Angew. Chem.* **2012**, *124*, 1800–1810; *Angew. Chem. Int. Ed.* **2012**, *51*, 1766–1776; f) J. Roncali, P. Leriche, P. Blanchard, *Adv. Mater.* **2014**, *26*, 3821–3838.
- [5] For examples of organic solar cells with discotic small molecules, see: a) L. Schmidt-Mende, A. Fechtenkötter, K. Müllen, E. Moons, R. H. Friend, J. D. MacKenzie, *Science* **2001**, *293*, 1119–1122; b) Y. Matsuo, Y. Sato, T. Niinomi, I. Soga, H. Tanaka, E. Nakamura, *J. Am. Chem. Soc.* **2009**, *131*, 16048–16050; c) A. A. Gorodetsky, C.-Y. Chiu, T. Schiros, M. Palma, M. Cox, Z. Jia, W. Sattler, I. Kymmissis, M. Steigerwald, C. Nuckolls, *Angew. Chem.* **2010**, *122*, 8081–8084; *Angew. Chem. Int. Ed.* **2010**, *49*, 7909–7912; d) T. Sagawa, S. Yoshikawa, H. Imahori, *J. Phys. Chem. Lett.* **2010**, *1*, 1020–1025.
- [6] a) G. M. Whitesides, E. E. Simanek, J. P. Mathias, C. T. Seto, D. N. Chin, M. Mammen, D. M. Gordon, *Acc. Chem. Res.* **1995**, *28*, 37–44; b) M. Mascal, N. M. Hext, R. Warmuth, M. H. Moore, J. P. Turkenburg, *Angew. Chem.* **1996**, *108*, 2348–2350; *Angew. Chem. Int. Ed. Engl.* **1996**, *35*, 2204–2206; c) L. J. Prins, D. N. Reinhoudt, P. Timmerman, *Angew. Chem.* **2001**, *113*, 2446–2492; *Angew. Chem. Int. Ed.* **2001**, *40*, 2382–2426; d) Y. Ma, S. V. Kolotuchin, S. C. Zimmerman, *J. Am. Chem. Soc.* **2002**, *124*, 13757–13769.
- [7] a) J. P. Mathias, E. E. Simanek, J. A. Zerkowski, C. T. Seto, G. M. Whitesides, *J. Am. Chem. Soc.* **1994**, *116*, 4316–4325; b) A. G. Bielejewska, C. E. Marjo, L. J. Prins, P. Timmerman, F. de Jong, D. N. Reinhoudt, *J. Am. Chem. Soc.* **2001**, *123*, 7518–7533.
- [8] P. A. Korevaar, S. J. George, A. J. Markvoort, M. M. J. Smulders, P. A. J. Hilbers, A. P. H. J. Schenning, T. F. A. De Gref, E. W. Meijer, *Nature* **2012**, *481*, 492–496.
- [9] a) S. Yagai, T. Kinoshita, Y. Kikkawa, T. Karatsu, A. Kitamura, Y. Honsho, S. Seki, *Chem. Eur. J.* **2009**, *15*, 9320–9324; b) S. Yagai, Y. Goto, X. Lin, T. Karatsu, A. Kitamura, D. Kuzuhara, H. Yamada, Y. Kikkawa, A. Saeki, S. Seki, *Angew. Chem.* **2012**, *124*, 6747–6751; *Angew. Chem. Int. Ed.* **2012**, *51*, 6643–6647.
- [10] S. Yagai, S. Kubota, H. Saito, K. Unoike, T. Karatsu, A. Kitamura, A. Ajayaghosh, M. Kanesato, Y. Kikkawa, *J. Am. Chem. Soc.* **2009**, *131*, 5408–5410.
- [11] S. Yagai, Y. Goto, T. Karatsu, A. Kitamura, Y. Kikkawa, *Chem. Eur. J.* **2011**, *17*, 13657–13660.
- [12] a) J. C. MacDonald, G. M. Whitesides, *Chem. Rev.* **1994**, *94*, 2383–2420; b) C.-C. Chu, G. Raffy, D. Ray, A. Del Guerzo, B. Kauffmann, G. Wantz, L. Hirsch, D. M. Bassani, *J. Am. Chem. Soc.* **2010**, *132*, 12717–12723; c) S. Yagai, Y. Nakano, S. Seki, A. Asano, T. Okubo, T. Isoshima, T. Karatsu, A. Kitamura, Y. Kikkawa, *Angew. Chem.* **2010**, *122*, 10186–10190; *Angew. Chem. Int. Ed.* **2010**, *49*, 9990–9994.
- [13] For examples of oligothiophene supramolecular systems, see: a) F. S. Schoonbeek, J. H. van Esch, B. Wegewijs, D. B. A. Rep, M. P. de Haas, T. M. Klapwijk, R. M. Kellogg, B. L. Feringa, *Angew. Chem.* **1999**, *111*, 1486–1490; *Angew. Chem. Int. Ed.* **1999**, *38*, 1393–1397; b) A. P. H. J. Schenning, A. F. M. Kilbinger, F. Biscarini, M. Cavallini, H. J. Cooper, P. J. Derrick, W. J. Feast, R. Lazzaroni, P. Leclerc, L. A. McDonell, E. W. Meijer, S. C. J. Meskers, *J. Am. Chem. Soc.* **2002**, *124*, 1269–1275; c) T. Yasuda, H. Ooi, J. Morita, Y. Akama, K. Minoura, M. Funahashi, T. Shimomura, T. Kato, *Adv. Funct. Mater.* **2009**, *19*, 411–419; d) K. Sugiyasu, S. Kawano, N. Fujita, S. Shinkai, *Chem. Mater.* **2008**, *20*, 2863–2865; e) W.-W. Tsai, I. D. Tevis, A. S. Tayi, H. Cui, S. I. Stupp, *J. Phys. Chem. B* **2010**, *114*, 14778–14786; f) I. D. Tevis, L. C. Palmer, D. J. Herman, I. P. Murray, D. A. Stone, S. I. Stupp, *J. Am. Chem. Soc.* **2011**, *133*, 16486–16494; g) D. A. Stone, A. S. Tayi, J. E. Goldberger, L. C. Palmer, S. I. Stupp, *Chem. Commun.* **2011**, *47*, 5702–5704.
- [14] F. C. Krebs, H. Spanggaard, *Sol. Energy Mater. Sol. Cells* **2005**, *88*, 363–375.
- [15] W. Li, T. Maddux, L. Yu, *Macromolecules* **1996**, *29*, 7329–7334.
- [16] a) N. Katsonis, H. Xu, R. M. Haak, T. Kudernac, Z. Tomovic, S. George, M. Van der Auweraer, A. P. H. J. Schenning, E. W. Meijer, B. L. Feringa, S. De Feyter, *Angew. Chem.* **2008**, *120*, 5075–5079; *Angew. Chem. Int. Ed.* **2008**, *47*, 4997–5001; b) J. A. A. W. Elemans, S. Lei, S. De Feyter, *Angew. Chem.* **2009**, *121*, 7434–7469; *Angew. Chem. Int. Ed.* **2009**, *48*, 7298–7332; c) K. Tahara, S. Lei, J. Adisojoso, S. De Feyter, Y. Tobe, *Chem. Commun.* **2010**, *46*, 8507–8525.
- [17] N. Katsonis, E. Lacaze, B. L. Feringa, *J. Mater. Chem.* **2008**, *18*, 2065–2073.
- [18] A. Miura, P. Jonkheijm, S. De Feyter, A. P. H. J. Schenning, E. W. Meijer, F. C. De Schryver, *Small* **2004**, *1*, 131–137.
- [19] C. A. Hunter, J. K. M. Sanders, *J. Am. Chem. Soc.* **1990**, *112*, 5525–5534.
- [20] The absence of helical morphology in the AFM image is not surprising because no clear helical gaps detectable by AFM should be generated on the surface of this type of columnar structures, which are organized through the stacking of rosettes with rotational displacement.
- [21] S. Gondo, Y. Goto, M. Era, *Mol. Cryst. Liq. Cryst.* **2007**, *470*, 353–358.
- [22] K. Sugiyasu, Y. Honsho, R. M. Harrison, A. Sato, T. Yasuda, S. Seki, M. Takeuchi, *J. Am. Chem. Soc.* **2010**, *132*, 14754–14756.
- [23] a) G. Yu, J. Gao, J. C. Hummelen, F. Wudl, A. J. Heeger, *Science* **1995**, *270*, 1789–1791; b) M. C. Scharber, D. Mühlbacher, M. koppe, P. Denk, C. Waldauf, A. J. Heeger, C. J. Brabec, *Adv. Mater.* **2006**, *18*, 789–794.
- [24] a) B. Walker, A. B. Tamayo, X.-D. Dang, P. Zalar, J. H. Seo, A. Garcia, M. Tantiwiwat, T.-Q. Nguyen, *Adv. Funct. Mater.* **2009**, *19*, 3063–3069; b) U. Mayerhöffer, K. Deing, K. Gruß, H. Braunschweig, K. Meerholz, F. Würthner, *Angew. Chem.* **2009**, *121*, 8934–8937; *Angew. Chem. Int. Ed.* **2009**, *48*, 8776–8779; c) S. Loser, C. J. Bruns, H. Miyachi, R. P. Ortiz, A. Facchetti, S. I. Stupp, T. J. Marks, *J. Am. Chem. Soc.* **2011**, *133*, 8142–8145;

- d) O. P. Lee, A. T. Yiu, P. M. Beaujuge, C. H. Woo, T. W. Holcombe, J. E. Millstone, J. D. Douglas, M. S. Chen, J. M. J. Fréchet, *Adv. Mater.* **2011**, *23*, 5359–5363; e) J. Zhou, X. Wan, Y. Liu, Y. Zuo, Z. Li, G. He, G. Long, W. Ni, C. Li, X. Su, Y. Chen, *J. Am. Chem. Soc.* **2012**, *134*, 16345–16351; f) T. Bura, N. Leclerc, S. Fall, P. Lévéque, T. Heiser, P. Retailleau, S. Rihm, A. Mirloup, R. Ziessel, *J. Am. Chem. Soc.* **2012**, *134*, 17404–17407; g) X. Liu, Y. Sun, L. A. Perez, W. Wen, M. F. Toney, A. J. Heeger, G. C. Bazan, *J. Am. Chem. Soc.* **2012**, *134*, 20609–20612; h) K. R. Graham, P. M. Wierszewski, R. Stalder, M. J. Hartel, J. Mei, F. So, J. R. Reynolds, *Adv. Funct. Mater.* **2012**, *22*, 4801–4813; i) Y. Liu, Y. Yang, C.-C. Chen, Q. Chen, L. Dou, Z. Hong, G. Li, Y. Yang, *Adv. Mater.* **2013**, *25*, 4657–4662.
- [25] For an exceptionally high PCE of 6.7% achieved at a relatively low annealing temperature (70 °C), see: Y. Sun, G. C. Welch, W. L. Leong, C. J. Takacs, G. C. Bazan, A. J. Heeger, *Nat. Mater.* **2012**, *11*, 44–48.
- [26] For high PCE over 4% without annealing, see: H. Bürckstümmer, E. V. Tulyakova, M. Deppisch, M. R. Lenze, N. M. Kronenberg, M. Gsänger, M. Stolte, K. Meerholz, F. Würthner, *Angew. Chem.* **2011**, *123*, 11832–11836; *Angew. Chem. Int. Ed.* **2011**, *50*, 11628–11632.
- [27] J. Zhao, A. Swinnen, G. V. Assche, J. Manca, D. Vanderzande, B. V. Mele, *J. Phys. Chem. B* **2009**, *113*, 1587–1591.
- [28] M. M. Wienk, J. M. Kroon, W. J. H. Verhees, J. Knol, J. C. Hummelen, P. A. van Hal, R. A. J. Janssen, *Angew. Chem.* **2003**, *115*, 3493–3497; *Angew. Chem. Int. Ed.* **2003**, *42*, 3371–3375.
- [29] a) A. El-ghayoury, A. P. H. J. Schenning, P. A. van Hal, J. K. J. van Duren, R. A. J. Janssen, E. W. Meijer, *Angew. Chem.* **2001**, *113*, 3772–3775; *Angew. Chem. Int. Ed.* **2001**, *40*, 3660–3663; b) C.-H. Huang, N. D. McCle-
naghan, A. Kuhn, J. W. Hofstraat, D. M. Bassani, *Org. Lett.* **2005**, *7*, 3409–3412; c) P. Jonkheijm, J. K. J. van Duren, M. Kemerink, R. A. J. Janssen, A. P. H. J. Schenning, E. W. Meijer, *Macromolecules* **2006**, *39*, 784–788; d) A. Wicklein, S. Ghosh, M. Sommer, F. Würthner, M. Thelakkat, *ACS Nano* **2009**, *3*, 1107–1114; e) R. B. K. Siram, K. Tandy, M. Horecha, P. Formanek, M. Stamm, S. Gevorgyan, F. C. Krebs, A. Kiriy, P. Meredith, P. L. Burn, E. B. Namdas, S. Patil, *J. Phys. Chem. C* **2011**, *115*, 14369–14376; f) H.-P. Fang, J.-W. Lin, I.-H. Chiang, C.-W. Chu, K.-H. Wei, H.-C. Lin, *J. Polym. Sci. Part A: Polym. Chem.* **2012**, *50*, 5011–5022; g) D. Patra, M. Ramesh, D. Sahu, H. Padhy, C.-W. Chu, K.-H. Wei, H.-C. Lin, *Polymer* **2012**, *53*, 1219–1228; h) R. J. Kumar, J. Subbiah, A. B. Holmes, *Beilstein J. Org. Chem.* **2013**, *9*, 1102–1110.
- [30] S. J. Kang, J. B. Kim, C.-Y. Chiu, S. Ahn, T. Schiros, S. S. Lee, K. G. Yager, M. F. Toney, Y.-L. Loo, C. Nuckolls, *Angew. Chem.* **2012**, *124*, 8722–8725; *Angew. Chem. Int. Ed.* **2012**, *51*, 8594–8597.
- [31] a) F. C. Grozema, L. D. A. Siebbeles, *J. Phys. Chem. Lett.* **2011**, *2*, 2951–2958; b) W. L. Rance, A. J. Ferguson, T. McCarthy-Ward, M. Heeney, D. S. Ginley, D. C. Olson, G. Rumbles, N. Kopidakis, *ACS Nano* **2011**, *5*, 5635–5646; c) A. Saeki, M. Tsuji, S. Seki, *Adv. Energy Mater.* **2011**, *1*, 661–669; d) A. Saeki, S. Yoshikawa, M. Tsuji, Y. Koizumi, M. Ide, C. Vijayakumar, S. Seki, *J. Am. Chem. Soc.* **2012**, *134*, 19035–19042.

Received: July 15, 2014

Published online on October 3, 2014